NEAR-FIELD ACOUSTICAL IMAGING USING LATERAL BENDING MODE OF ATOMIC FORCE MICROSCOPE CANTILEVERS

Applications to fracture mechanics of NC-Zirconia

A. Caron, U. Rabe, J. Rödel, W. Arnold

Fraunhofer-Institute for Non-Destructive Testing (IZFP), Bldg. 37, University, D-66123 Saarbrücken, Germany; Institute of Materials Science, University of Technology, Darmstadt, D-64287 Darmstadt, Germany

Abstract: Scanning probe microscopy techniques enable one to investigate surface properties such as contact stiffness and friction between the probe tip and a sample with nm resolution. So far the bending and the torsional eigenmodes of an atomic force microscope cantilever have been used to image variations of elasticity and shear elasticity, respectively. Such images are near-field images with the resolution given by the contact radius typically between 10 nm and 50 nm. We show that the flexural modes of a cantilever oscillating in the width direction and parallel to the sample surface can also be used for imaging. Additional to the dominant in-plane component of the oscillation, the lateral modes exhibit a vertical component as well, provided there is an asymmetry in the cross-section of the cantilever or in its suspension. The out-of-plane deflection renders the lateral modes detectable by the optical position sensors used in atomic force microscopes. We studied cracks which were generated by Vickers indents, in submicro- and nanocrystalline ZrO_2. Images of the lateral contact stiffness were obtained by vibrating the cantilever close to a contact-resonance frequency. A change in contact stiffness causes a shift of the resonant frequency and hence a change of the cantilever vibration amplitude. The lateral contact-stiffness images close to the crack faces display a contrast that we attribute to altered elastic properties indicating a process zone. This could be caused by a stress-induced phase transformation during crack propagation. Using the contact mode of an atomic force microscope, we measured the crack-opening displacement as a function of distance from the crack tip, and we determined the crack-tip toughness K_{tip}. Furthermore, K_{1c} was inferred from the length of radial cracks of Vickers indents that were measured using classical scanning acoustic microscopy

Key words: Atomic Force Microscopy; Atomic Force Acoustic Microscopy; Scanning Acoustic Microscopy; Crack-tip toughness; Process zone

M.P. André (ed.), Acoustical Imaging, 31–41.

1. INTRODUCTION

The Atomic Force Microscope (AFM) [1] has found wide applications in biology, physics and material science. Most AFM operation modes measure the deflection of the cantilever caused by the forces acting between the tip and the sample while it is scanned. This allows mapping of surface properties such as topography, elasticity, magnetic or piezoelectric domains and other quantities with nm resolution. Forces lateral and normal to the sample surface contribute to the total tip-sample interaction [2]. In friction force microscopy lateral tip-sample forces are measured [3]. In early experiments the lateral deflection of a bent tungsten wire [4] or the buckling of the cantilever in its length direction [5] were exploited to image atomic-scale friction. In commercial instruments friction and lateral forces are detected by measuring the torsion of AFM cantilevers. In a recent publication we showed that the lateral bending modes of an AFM cantilever can be used for imaging variations of shear elasticity [6] in the so-called atomic force acoustic microscopy mode (AFAM) [7]. Here we present results on the measurement of the crack-tip toughness of submicro- and nanocrystalline stabilized zirconia. For this purpose the crack opening displacement (COD) was measured, using a commercial AFM (Dimension 3000 from Veeco/DI S. Barbara). The purpose of this work was to determine whether stress-induced phase transformation of stabilized zirconia still occurs at small grain sizes. Therefore AFAM images have been recorded along the crack and at its tip in order to quantify the extension of the process zone.

1.1 Fracture Mechanics

The theory of Griffiths' fracture mechanics postulates that crack propagation in materials occurs when the elastic work provided equals the energy to create two new surfaces [8]. This is expressed by the following equation:

$$G_c = \frac{dU}{dc} = 4\gamma_0 \tag{1}$$

where G_c is the energy release per crack increment, dU is the energy supplied to the system, dc is the crack extension per unit width, and γ_0 is the surface energy. In some technical ceramics like SiC, Al_2O_3, and ZrO_2 energy-dissipative processes take place that occur simultaneously when a crack propagates. Such processes consume energy and are thus responsible for an increase of G_c. In such cases one speaks of resistance curve (R-curve)

behavior [9]. For example coarse-grained Al_2O_3 exhibits a typical resistance curve for G_c versus crack propagation [10]. Two effects contribute to this behavior of Al_2O_3. Firstly the friction caused by serrated crack-walls and secondly micro-cracks generated in a process zone [10, 11]. In order to take the contribution of energy dissipative processes into account, Eq. 1 has to be extended by a further term:

$$G_c = R_0 + R_\mu = 2\gamma_0 \tag{2}$$

Here, R_0 and R_μ are the intrinsic contribution and the contribution of energy-dissipative processes to the total fracture energy R, which balances the mechanical energy release per crack increment G_c.

Zirconia undergoes a reversible martensitic transformation from the tetragonal high-temperature to the monoclinic phase. The phase transformation starts in pure zirconia at 1220 °C and ends at 600 °C. This transformation is associated with a volume strain of 4% and a deformation of 16%. Alloying with stabilizing elements like MgO, YO_2, CaO or CeO_2 enables one to adjust the transformation-starting temperature in such a way that the high-temperature phase is still metastable at room temperature. This stabilized phase can then experience a stress-induced martensitic transformation at room temperature. Thermodynamics delivers a critical grain size D_c under which the phase transformation can no longer occur [12]:

$$D \geq D_c = 6\left(\gamma_m - g_s\gamma_t\right) \Big/ \left[\left|\Delta G^c\right| - \Delta U_{se}\right] \tag{3}$$

Here $\gamma_{m,t}$ are the surface energies for the monoclinic phase and the tetragonal one respectively, g_s is the ratio of the surfaces of the tetragonal to the monoclinic particles, ΔG^c is the chemical free energy, and ΔU_{se} is the deformation energy associated with the phase transformation.

With the emergence of new polycrystalline materials with grain sizes in the sub-micrometer and nanometer range and the importance of the energy-dissipative phase transformation for fracture-toughness enhancement, the grain size effect becomes crucial. As it is difficult to determine the necessary thermodynamical quantities, measurements of the critical grain size remains the only way to obtain an optimal microstructure.

For the investigation of the fracture processes the crack-opening displacement was measured. This method follows from Irwin's work on stress concentration at a crack tip [13]. The crack-opening displacement (Fig. 1) profile has a parabolic shape if no closure stresses are present close to the crack tip [14]:

$$u(x) = u_y(x) = \frac{K_{tip}}{E'}\left(\frac{8x}{\pi}\right)^{1/2}, \quad (x > 0) \tag{4}$$

Here, x is the distance from the crack tip, $E' = E/(1-\upsilon^2)$ is the reduced Young's modulus, and K_{tip} is the crack-tip toughness at the crack tip. In the case where a stress-induced transformation takes place parallel to crack propagation, closure-stresses emerge in the vicinity of the crack tip as a consequence of the strain associated with the transformation. Then the plot of the crack opening deviates from the parabolic shape. From such a deviation it is possible to quantify the closure stresses [15].

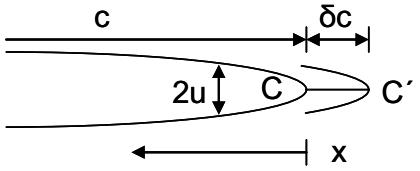

Figure 1. Definition of the crack-opening displacement (COD) u(x). The path CC' symbolizes an incremental crack extension δc of unit width, see [14].

Furthermore the fracture toughness can be determined by measuring the length c_{rad} of the so-called radial cracks in a Vickers indent [16]:

$$K_{1c} = 0.067\left(c_{rad}/a\right)^{-3/2} Ha^{-1/2}\left(H/E\right)^{2/5} \tag{5}$$

Here, 2a is the diagonal of the Vickers indent, $H = F/2a^2$ is the hardness and E is Young's modulus. Eq. 5 is valid under the assumption that a half-penny shaped crack forms under the indentation zone, which is an idealization for materials exhibiting transformation toughening.

2. EXPERIMENTAL METHODS

In this work several microscopy techniques have been used for investigating the toughness and the crack-tip toughness. Crack opening profiles have been measured by means of AFM in contact mode and by measuring the length of the radial cracks of the Vickers indent using scanning acoustic microscopy [17]. Employing AFAM, imaging of the process zone in the vicinity of cracks has been carried out.

The AFM measurements were carried out with a Dimension 3000 from Digital Instruments/Veeco [18]. In the contact mode of AFM operation, the sharp sensor tip at the end of a micro-fabricated elastic beam is scanned over the sample surface. The tip radius is a few tens of nm, the contact radius, however, typically remains below 10 nm. The interaction forces between sensor tip and sample surface cause a deflection of the cantilever which is measured with a position-sensitive photo-diode. If the deflection of the cantilever and thus the interaction forces are kept constant by a feedback

loop, the topography of the sample surface can be measured with a nanoscale resolution. This allows one to follow the contour of cracks and to measure the COD and compare it to the theoretically expected curve (Eq. 4).

In AFAM the resonances of the cantilever are excited by using an ultrasonic transducer coupled to the sample [7], or by using a piezoelectric element mounted in the cantilever holder [19]. In contact with the sample surface the resonance frequency of the cantilever is determined by the contact stiffness between sensor tip and sample, which represents one of the two boundary conditions of the cantilever eigenmode. The contact stiffness is in turn determined by the elastic properties of the investigated sample. AFAM can be operated in two different working modes. In the spectroscopic mode resonance spectra are collected at one point of the surface from which the indentation modulus of the sample and information on friction can be gained [2, 7]. In this work the imaging mode of AFAM has mainly been used. In this mode a fixed frequency is chosen next to the resonance frequency. Due to local variations of the contact stiffness the resonance frequency shifts, so that the oscillation amplitude of the cantilever changes. The amplitude is then digitized and plotted as an image. Unlike in the spectroscopic mode, the information gained with this method is only qualitative regarding the elastic properties of the sample.

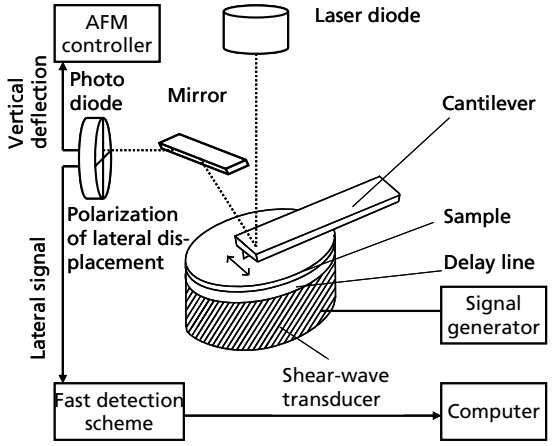

Figure 2. Principle of an atomic force acoustic microscope using lateral bending modes.

In earlier work of AFAM, bending modes have been excited by injecting longitudinal ultrasonic waves through the sample causing out-of-plane displacements of the surface [2, 7, 20]. Furthermore, torsion modes of the cantilever can be excited and used for friction investigation [2, 21]. Torsion modes can be excited by using a shear-wave transducer with its polarization perpendicular to the length axis of the cantilever. Recently we measured the vibration spectra of cantilevers made of single silicon crystal by using an optical scanning interferometer. We found that eigenmodes of the cantilever

can be excited by in-plane displacements, which are neither *torsional nor flexural* modes [6] (Fig. 2). Furthermore, this mode has been characterized regarding its sensitivity to variations of elastic stiffness [6].

3. SAMPLES AND PREPARATION

Sub-microcrystalline zirconia stabilized with 3 mol% Y_2O_3 was investigated in order to measure the crack-tip toughness. Two samples with different mean grain sizes (500 nm and 98 nm) were prepared in order to observe the influence of the grain size on the martensitic transformation and on the crack-tip toughness. The samples were ground with SiC abrasive paper and polished with a diamond suspension with a particle size down to 0.25 μm. A final polish with alumina particles again of 0.25 μm size was used to reveal the grain structure.

For the crack initiation a Vickers indent with a load of ~ 200 N was made. For the separate hardness measurements a micro-indenter from Leica, type VMHT Mot was used. In order to avoid parallel crack initiation, the loading forces were kept small (4.9 N and 9.8 N).

4. MEASUREMENTS AND DISCUSSION

Fig. 3 and 4 show the COD measured with the AFM as a function of the distance to the crack tip for both samples. As concerns the sample having a mean grain size of 98 nm, several cracks were measured, whereas in the case of the sample with 500 nm mean grain size one crack was measured at different times after indentation. For evaluating the COD according to Eq. 4 the Young's modulus of zirconia was assumed to be 210 GPa and its Poisson ratio 0.29. The crack-tip toughness slightly decreases with grain size from 4.1 to 3.2 $\mathrm{MPa}\sqrt{\mathrm{m}}$, with decreasing grain size from 500 nm to 98 nm. This result can be compared with measurements of the crack-opening displacement, using a high-resolution electron microscope where values of 2.8 to 2.3 $\mathrm{MPa}\sqrt{\mathrm{m}}$ were obtained for the large and the smaller grain size, respectively [22]. The crack-tip toughness is altered by phase transformation due to shear stresses, whereas the phase transformation due to dilatational stresses affects the shielding term R_μ. The difference between both types of samples occurs as the phase transformation is restrained at a smaller grain size. Moreover, the deviation of the crack opening profiles from the parabolic shape supports this explanation. This effect is still more remarkable with the sample of 500 nm mean grain size (Fig. 4). Fig. 4 also includes the time dependence of the crack-tip toughness. Sub-critical crack

growth leads to a small contribution to crack propagation, which unloads the crack tip and provides a smaller crack-tip stress-intensity factor, albeit with a small effect only.

For comparison, the fracture toughness was also determined by measuring the length of the radial cracks c_{rad} of the Vickers indent in scanning acoustic microscope images (ELSAM, Leica, Wetzlar, Germany) at a frequency of 1 GHz (Fig. 5). From the images the radial crack length c_{rad}, the size 2a of the Vickes indent, and the hardness H were determined in order to calculate K_{1c} from Eq. 5. For the sample with a grain size of 98 nm the following values were obtained from the images: 2a = 162 (± 8) µm, 2_{crad} = 422 (± 8) µm. This leads to a hardness of H = 14.9 (± 1.5) GPa and a value of 1400 (± 140) for the Vicker hardness using the standard definition for HV. With these data, a value of $K_{1c}= 3.7 \pm 0.26$ MPa$\sqrt{m}$ is obtained. As discussed elsewhere [22], a very small grain size in 3-YTZP over stabilizes the tetragonal crystal structure, such that very little transformation toughening occurs and fracture toughness and crack tip toughness almost coincide.

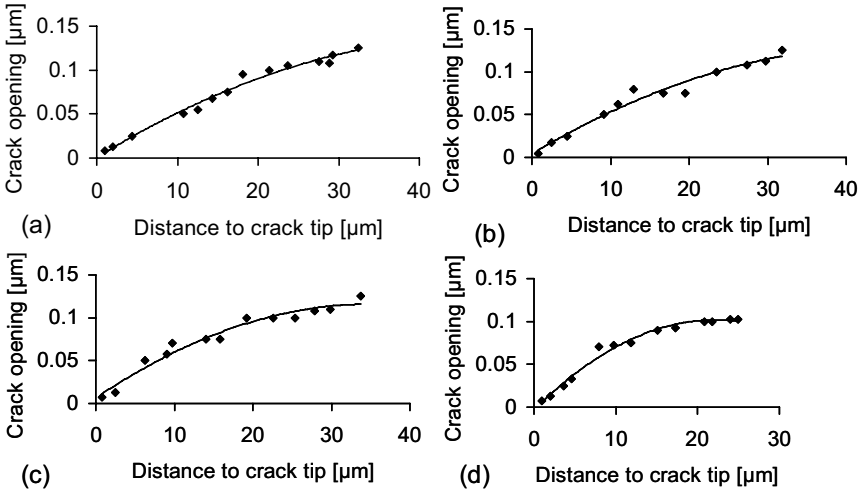

Figure 3. COD u(x) for different cracks on the 3Y-ZrO_2 sample with 98 nm mean grain size. Eq. 4 delivers a crack-tip toughness K_{tip} = 3.15 MPam$^{1/2}$ averaged over all profiles.

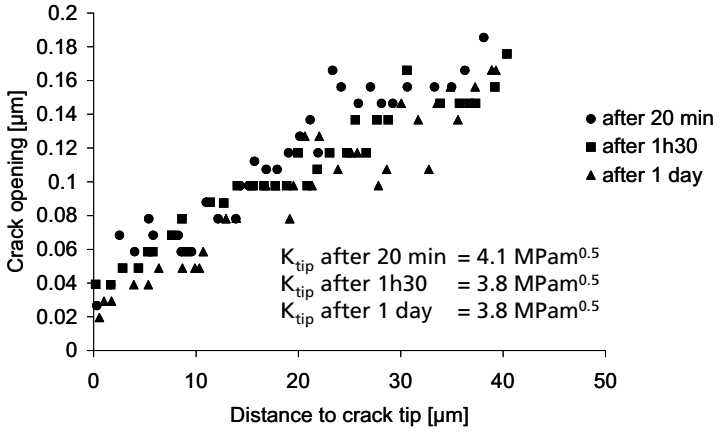

Figure 4. Crack opening displacement as a function of the distance to the crack tip and of the time for the 3Y-ZrO_2 sample with 500 nm mean grain size.

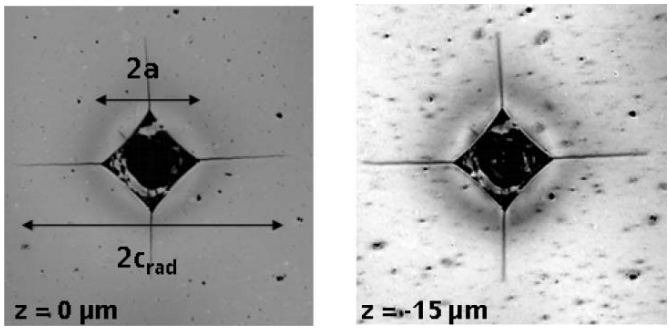

Figure 5. Scanning acoustic microscopy images of a Vickers indent in the zirconia sample with 98 nm grain size at two different defocusing distances z. The indent was made with a loading force of 196.2 N. K_{1c} is obtained from the radial crack length c_{rad} whose apparent length became slightly larger with decreasing z. Images size is 500×500 µm^2.

Table 1. Results of the crack-tip toughness of 3Y-ZrO_2 with tow different grains sizes.

Grain size	Measuring technique	Hardness [GPa]	$K_{tip,}$ K_{Ic}, [MPa$\sqrt{m}$]
98 nm	COD		3.15 ± 0.15
500 nm	COD		4.1 ± 0.20
98 nm	SAM	14.9 ± 1.5	3.67 ± 0.26
98 nm	SEM		2.3
500 nm	SEM		2.8

A further aim of this work was to quantify the width of the process zone in the vicinity of the crack tip and thus to measure the extension of the closure stress-field caused by the stress-induced phase transformation (Table 1). On

the sample with 500 nm mean grain size we observed a depression of the topography close to the crack walls (Fig. 6(a)) and of the crack tip. This depression is connected to the deformation associated with the martensitic transformation. By measuring this topography contrast, the process zone was estimated to be 600 nm wide and about 15 nm deep. Parallel to the topography image, AFAM images using the first contact bending mode (f = 349 kHz) and the first contact lateral bending mode (f = 676 kHz) of a cantilever with stiffness 1.7 N/m were recorded at the same location. The image obtained, using the first contact bending mode, does not show a direct correlation with the topography contrast which could be associated with a process zone. The lateral bending mode seems to be more sensitive in this case. Indeed a band of higher amplitude along the crack fronts can be observed which coincides with the depression observed in topography image (see Figs. 6(b), 6(c)). This implicates a change of the shear elastic properties in the vicinity of the crack. Figs. 6(b) and 6(c) reveal different contrasts in the grain structures. In Fig. 6(c) the grain structure is far better resolved. We believe that the difference between both images is caused by the fact that by using a bending mode local variations of the indentation modulus $M = E/(1-\upsilon^2)$ [7, 20] are emphasized, whereas by using a lateral bending mode local variations of the shear modulus G become more pronounced in the contrast. At the moment we assume that in zirconia the anisotropy of the shear modulus is larger than the anisotropy of the indentation modulus.

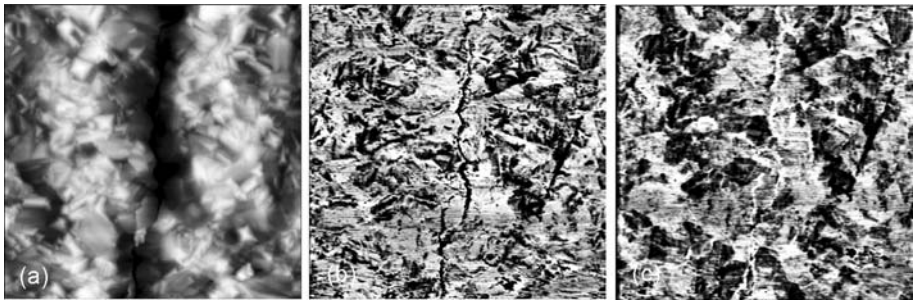

Figure 6. (a) AFM topography image of a crack in a 3Y-ZrO_2 sample with 500 nm mean grain size (z-scale: 70 nm); (b) AFAM image at the same place using the first contact bending mode (f = 349 kHz). Parallel to the crack walls there is a bright contrast indicating the change in shear elasticity; (c) AFAM image at the same location using the first contact lateral bending mode (f = 676 kHz). The static load was 147 nN in all three images; Size: 5×5 μm².

5. CONCLUSION

The influence of the grain size on the crack-tip toughness of zirconia and thus on the stress-induced martensitic transformation was verified on two samples with different mean grain sizes (98 nm and 500 nm) since the crack-tip toughness is slightly smaller for the zirconia sample having the smaller grain size. This can be explained by the restriction of the process zone at the smaller grain size. Furthermore, a process zone could be identified with contact atomic force microscopy and also by atomic force acoustic microscopy using the first *lateral* bending mode in contact. The contrast in this new imaging mode depends on the surface shear elasticity. Finally quantitative measurements of the crack-tip toughness K_{tip} were made by measuring the crack-opening displacement with an AFM revealing a grain-size dependence. The fracture toughness was determined by measuring the radial crack-length of Vickers indents with a scanning acoustic microscope. Future measurements are planned in order to determine the critical grain size above which the phase transformation sets in.

REFERENCES

1. G. Binnig, C.F. Quate, and Ch. Gerber, “Atomic Force Microscope”, Phys. Rev. Lett., **56**, 930 (1986).
2. V. Scherer, M. Reinstädtler, and W. Arnold, “Atomic Force Microscopy with Lateral Modulation” in *Applied Scanning Probe Methods*, Eds. H. Fuchs, B. Bhushan, and S. Hosaka (Springer, Berlin, 2003), pp. 76–115, and references therein.
3. B. Bhushan, in *Handbook of Nanotechnology*, edited by B. Bhushan (Springer, Berlin, 2004), pp. 497ff, and references therein.
4. C.M. Mate, G.M. McClelland, R. Erlandsson, and S. Chiang, “Atomic-scale friction of a tungsten tip on a graphite surface”, Phys. Rev. Lett., **59**, 1942 (1987).
5. T. Göddenhenrich, S. Müller, and C. Heiden, “A lateral technique for simultaneous friction and topography measurements with the atomic force microscope”, Rev. Sci. Instrum., **65**, 2870 (1994).
6. A. Caron, U. Rabe, M. Reinstädtler, J.A. Turner, and W. Arnold, “Imaging using lateral bending modes of atomic force microscope cantilevers”, Appl. Phys. Lett. **85**, 6398 (2004).
7. U. Rabe, S. Amelio, E. Kester, V. Scherer, S. Hirsekorn, and W. Arnold, “Quantitative Determination of Contact Stiffness Using Atomic Force Acoustic Microscopy”, Ultrasonics, **38**, 430 (2000), and reference contained therein.
8. A.A. Griffiths, “The Phenomena of Rupture and Flaw in Solids”, Phil. Trans. R. Soc. London, **A221**, 163 (1920).
9. T.L. Anderson, Fracture Mechanics - Fundamentals and Applications, Chapter 6: Fracture Mechanics in Nonmetals, Boston: CRC Press (1991).
10. E. Babilon, G. Kleist, R.W. Steinbrech, and H. Nickel, “Untersuchung von Mikrorissfeldern in der Umgebung eines Makrorisses in Al_2O_3-Keramik mittels der Röntgenkleinwinkelstreuung”, *Konferenzberichte des FZ Jülich*, 7, Eds. H. Nickel and R.W. Steinbrech, 175 (1991).

11. W. Arnold, G. Weides, and S. Faßbender "Measurement of Elastic Properties Related to the R-Curve-Behavior of Ceramics", *Proc. Asian Pacific Conf. Fract. & Strength 2001 and Int. Conf. Adv. Technol. in Exp.. Mech.*, Jap. Soc. of Mech. Eng., Tokyo, 2001, 517.
12. F.F. Lange, "Transformation Toughening. Part 1: Size Effects Associated with the Thermodynamics of Constrained Transformations", J. Mat. Sci., **17**, 225 (1982).
13. G.R. Irwin, "Fracture", *Handbuch der Physik*, Springer Verlag, Berlin, **6**, 551, (1958).
14. B.R. Lawn, "Fracture of Brittle Solids – Second Edition", *Sol. State Sci. Ser*. Cambridge University Press, (1993).
15. J. Rödel, G. Kelly, and B.R. Lawn, "In-Situ Measurements of Bridged Cracked Interfaces in the SEM", J. Am. Ceram. Soc., **73**, 3313 (1990).
16. D. Munz, and T. Fett, Mechanisches Verhalten keramischer Werkstoffe, in *Werkstoffforschung und –Technik*, B. Ilschner (Ed.), Springer, Heidelberg, 1989.
17. G.A.D. Briggs, "*Scanning Acoustic Microscopy*", Oxford University Press, 1992.
18. AFM – Digital Instrument, www.veeco.com.
19. K. Yamanaka, H. Ogiso, and O. Kosolov, "Analysis of Subsurface Imaging Effect of Contact Elasticity in the Ultrasonic Force Microscopy", Jpn. J. Appl. Phys., **33**, 3197 (1994).
20. M. Kopycinska-Müller, M. Reinstädtler, U. Rabe, A. Caron, S. Hirsekorn, and W. Arnold, "Ultrasonic modes in atomic force microscopy", *Proc. 27th Int. Symp. Acoustical Imaging*, Kluwer Plenum Press, Eds. W. Arnold and S. Hirsekorn, 699–704 (2004).
21. M. Reinstädtler, U. Rabe, V. Scherer, U. Hartmann, A. Goldade, B. Bhushan, and W. Arnold, "On the nanoscale measurement of friction using atomic force microscope cantilever torsional resonances", Appl. Phys. Lett., **82**, 2604 (2003).
22. J. Eichler, "Mechanical Properties of Nanocrystalline Zirconia", Ph.D. Thesis, Fachbereich Material- und Geowissenschaften, University of Technology, Darmstadt, Germany (2004).